crystals

MDPI

Article

Preliminary Parametric Investigations into Macro-Laser Polishing of Laser-Directed Energy Deposition of SS 304L Bulk Structures

Vijay Kumar Saini [1], Jinoop Arackal Narayanan [2,*], Niraj Sinha [1] and Christ Prakash Paul [3,4,*]

[1] Department of Mechanical Engineering, Indian Institute of Technology Kanpur, Kanpur 208016, Uttar Pradesh, India; saini.vijay31@gmail.com (V.K.S.); nsinha@iitk.ac.in (N.S.)
[2] School of Computing, Engineering & Digital Technologies, Teesside University, Middlesbrough TS1 3BX, UK
[3] Additive Manufacturing Technology Laboratory, Raja Ramanna Centre for Advanced Technology, Indore 452013, Madhya Pradesh, India
[4] Homi Bhabha National Institute, Anushaktinagar, Mumbai 400094, Maharashtra, India
* Correspondence: anjinoop@gmail.com (J.A.N.); paulcp@rrcat.gov.in (C.P.P.); Tel.: +44-(0)-1642342411 (J.A.N.); +91-731-2488396 (C.P.P.)

Abstract: The higher surface roughness of laser-directed energy deposition (LDED)-built components necessitates advanced and sustainable surface quality enhancement techniques like laser polishing. In the present work, a parametric study involving experimental investigation and numerical analysis is conducted to determine the effect of macro-laser polishing on LDED-built SS 304L structures. A thermophysical model is developed to simulate the effect of laser power and scan speed on the melt pool depth of the LDED-built samples. The simulated melt pool depth is compared with experimental results and is found to be in good agreement. Further, the correlation between the melt pool depth and surface behaviour is studied based on shallow surface melting and shallow over-melting mechanisms. A maximum reduction in surface roughness from 21.3 µm to 9 µm (~57%) is achieved with laser polishing, and process parameters' effect on the surface roughness is investigated. Scanning electron microscopy (SEM), energy-dispersive spectroscopy (EDS) mapping, and X-ray diffraction (XRD) are used to further characterize the laser-polished surface. SEM-EDS analysis shows that the segregation is more evident in laser-polished samples, while the XRD results indicate the absence of phase change during the process. This study paves the way to a greater understanding of the effect of macro-laser polishing on LDED-built SS 304L structures.

Keywords: laser-directed energy deposition; laser polishing; process parameters; surface roughness; characterization

check for updates

Citation: Saini, V.K.; Arackal Narayanan, J.; Sinha, N.; Paul, C.P. Preliminary Parametric Investigations into Macro-Laser Polishing of Laser-Directed Energy Deposition of SS 304L Bulk Structures. *Crystals* **2023**, *13*, 1604. https://doi.org/10.3390/cryst13111604

Academic Editor: Liangchi Zhang

Received: 21 October 2023
Revised: 13 November 2023
Accepted: 17 November 2023
Published: 20 November 2023

Copyright: © 2023 by the authors. Licensee MDPI, Basel, Switzerland. This article is an open access article distributed under the terms and conditions of the Creative Commons Attribution (CC BY) license (https://creativecommons.org/licenses/by/4.0/).

1. Introduction

Laser Additive Manufacturing (LAM) is the process of joining materials using high-power lasers to make objects from 3D model data using layer-upon-layer methodology. LAM can build components with complex geometry and tailored density/properties with reduced lead time [1,2]. LAM is mainly achieved using two methods: laser powder bed fusion (LPBF) and laser-directed energy deposition (LDED) [3]. In LPBF, the powder particles are spread over the powder bed and the moving laser impinges on the powder particles, leading to particle melting and fusion [4,5]. LDED, on the other hand, uses a high-power laser to create a melt pool on a build plate onto which feedstock material is added. The deposition takes place in a layer-by-layer fashion to build 3D components [3]. LPBF is attractive for building components with high design complexity, thin features, and lightweight designs, while LDED is commonly used to build functionally graded materials, near-net-shaped complex components and large-area clad and for the repair of engineering components [6].

Recently, LDED has been used by industries for building large-size engineering components [7]. However, this process is limited by the presence of porosity, residual stresses, cracks and distortions and high surface roughness [8]. One of the major limitations of LDED parts that restricts the direct deployment of the process for several engineering applications is the high surface roughness. The average surface roughness (Ra) obtained from conventional machining (like grinding and milling) is typically 1–2 µm, whereas the Ra value of LDED parts is in the range of 10–30 µm [2]. High surface roughness also affects the dimensional accuracy of the parts and limits the deployment of the technology. In addition, parts with a rough surface finish tend to have low fatigue resistance, making LDED unsuitable for applications where good mechanical performance against dynamic loading is required. Therefore, LDED-built components need to be subjected to surface finishing operations before their final usage.

One of the most advanced techniques for improving the surface finish of LDED-built components is laser polishing [9]. During laser polishing, the surface that comes in contact with the laser melts and the melted material relocates from peaks to valleys due to the action of surface tension, leading to improved surface quality [9]. In addition to improving the surface finish, laser polishing modifies the metallurgical characteristics at the polished zone. Laser polishing is environmentally friendly as compared to conventional polishing processes, which use abrasives and chemicals that are uneconomical and harmful to the operator as well as to the environment [10]. This process can be automated and can be used to polish hard materials and/or components with complex features, which makes its deployment in the aeronautical and automotive industries attractive [10]. Although conventional machining can achieve smoother surfaces, the advantages of laser polishing, such as reduced material loss in terms of chips, greater environmental friendliness, and decreased chemical usage, are drawing more attention to this technique.

Various researchers have reported the laser polishing of LAM-built components, and the majority of the research deals with process parameter optimization for improving the surface roughness. Ermergen and Faylan [11] attempted to study the effect of process parameters, like scanning speed, pulse duration, and laser power, on surface quality and observed that using adequate laser power, spot diameter, and pulse duration settings can increase surface quality. Marimuthu et al. [12] found that excessive thermal energy can result in carbonization and oxidation. Surface roughness depends on melt pool velocity, which in turn depends on laser power and scan speed. Krishnan et al. [10] emphasized the effect of laser polishing processes such as surface oxidation and carbonization. Laser polishing may provide a glossy surface finish if the laser parameters, such as energy density, spot diameter, and beam intensity, are precisely regulated. Dadbakhsh et al. [13] applied the design of experiments (DOE) for the laser polishing of LDED-built Inconel-718 and reduced the surface roughness of the sample to 80% of the initial surface roughness. Hafiz et al. [14] studied the effect of overlap between the laser beam tracks on the surface quality of AISI H13 tool steel during laser polishing. It was found that Ra was reduced by 65% for an overlap of 80% and reduced by 77.9% for an overlap of 95%, but a reduction in surface quality was only found after a 97.5% overlap. An overlap percentage of 95% reduced both the roughness and waviness of the material. Souza et al. [15] studied the surface characteristics and wettability of laser-polished SS 316L samples built using LDED. A reduction of up to 86% in Sa was observed and the Sz/Sa ratio was modified.

It can be observed from the open literature that there are limited parametric studies available on the laser polishing of LDED structures combining experimental and numerical analysis. Further, there is limited published literature on the effect of macro-laser polishing process parameters on melt pool geometry, surface topography, and material characteristics. Thus, in the present work, a systematic investigation was carried out to establish the effect of laser polishing parameters on the melt pool geometry, surface roughness, surface topography, and material characteristics of LDED-built SS 304L bulk structures. The major objective of the investigation was to determine the effect of variation in the process parameters on melt pool depth and surface roughness and evaluate the variation in surface

roughness with melt pool depth and laser energy per unit length according to experimental and simulated results. Also, the investigation was carried out to establish the effect of laser polishing parameters on the surface topography and material characteristics of LDED-built SS 304L bulk structures.

2. Materials and Methods

SS 304L powder with particles 45–106 microns in size was used for LDED deposition. The composition of the powder as provided by the powder manufacturer is presented in Table 1. An in-house developed 2 kW fibre-laser-based LDED system was used for depositing SS 304L bulk structures. It consisted of a glove box with a 5-axis manipulator, computer numerical controller, coaxial nozzle, and twin powder feeder. Figure 1a shows a schematic of the LDED system used for depositing SS 304L structures. More details about the system are reported in one of our previous research projects [16]. The process parameters yielding crack-free and continuous deposition of single tracks were selected for building bulk structures. The laser power, powder feed rate, scan speed, spot diameter, and track overlap used to build bulk SS 304L structures were 900 W, 8 g/min, 0.5 m/min, 2.5 mm, and 50%, respectively.

Table 1. Chemical composition of SS 304L powder.

Element	Composition (Wt.%)
Carbon	0.01
Manganese	0.8
Silicon	0.4
Chromium	18
Nickel	9
Iron	Balance

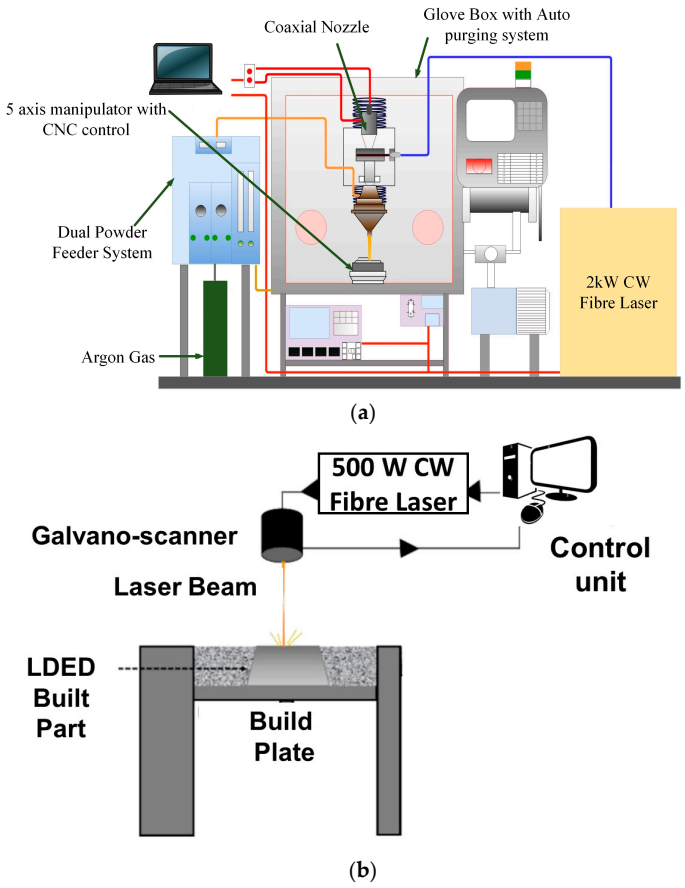

Figure 1. Schematic of (**a**) LDED and (**b**) laser polishing system.

An in-house developed continuous-wave fibre-laser-based LPBF system with a maximum laser power of 500 W was used for the laser polishing experiments. Laser polishing experiments were carried out by turning off the powder spreading in the LPBF system. The LPBF setup was used to deploy the faster scanning speed and smaller beam diameter required for laser polishing experiments. The laser direction for polishing was along the length of the workpiece. More details about the system are provided elsewhere [17]. Figure 1b presents a schematic of the modified LPBF system for laser polishing experiments. The experiments were performed by varying laser power and scan speed at a constant overlap percentage (50%) and spot diameter (500 μm). The process parameter settings and corresponding laser energy per unit length (LEL) are presented in Table 2 as per the Taguchi L9 array. LEL is defined as the ratio between laser power divided by scan speed [14].

$$\text{LEL} = \text{P}/\text{V} \quad (1)$$

where P is laser power and V is scan speed.

Table 2. Laser polishing parameters and corresponding LEL.

Sample Number	Laser Power (W)	Scan Speed (mm/s)	LEL (J/mm) [P/V]
Sample 1	100	300	0.33
Sample 2	100	500	0.2
Sample 3	100	700	0.142
Sample 4	150	300	0.5
Sample 5	150	500	0.3
Sample 6	150	700	0.214
Sample 7	200	300	0.66
Sample 8	200	500	0.4
Sample 9	200	700	0.285

A 3D optical profilometer from Bruker Contour GT-K was used to evaluate the surface roughness. The 3D roughness of the maximum area was determined by using the in-built stitching method, and the standard parameters used for measurement were as follows: back length, 15 μm; depth, 200 μm; stitching width, 5 mm; stitching height, 1.5 mm; and threshold, 1%. A Carl Zeiss scanning electron microscopy attached with an energy-dispersive spectroscopy (EDS) system from Oxford instruments was used for surface composition and topography studies. X-ray diffraction of the sample surface was performed with the help of Bruker D8 Focus with a step size of 0.02 degrees from 40 to 80°. The Scherrer equation was used to estimate the crystallite size from the XRD data with different sets of laser polishing parameters [6,17]. In order to measure the melt pool depth, the samples were epoxy-mounted, polished, and etched. Etching was carried out using Glyceregia (15 cc HCl + 10 cc Glycerol + 5 cc HNO_3) by immersing the samples in the solution for 90–120 s. A Nikon Eclipse LV100 industrial microscope was used for measuring the melt pool depth. Melt pool depth was measured at three different locations, and then the average value was recorded.

3. Numerical Modelling

A numerical model was developed to establish the effect of laser power and scan speed during the laser polishing of the LDED-built surface. The following assumptions were made for the simplification of the analysis:

(a) The material is isotropic and homogeneous;
(b) During melting and solidification, the flow of the melt pool is neglected;
(c) No chemical reaction takes place due to argon shielding;
(d) The laser beam intensity profile is Gaussian;
(e) The effect of evaporation, spattering, and balling is neglected.

A 3D heat transfer equation (refer to Equation (2)) [18] was used to compute the temperature distribution throughout the whole 3D domain, where ρ, C_p, T, v, and Q represent density, specific heat, the temperature of the workpiece, scan speed, and absorbed heat, respectively.

$$\rho C_p \frac{dT}{dt} + \rho C_p v \nabla T = \nabla(k \nabla T) + Q \quad (2)$$

The heat flux distribution when moving the Gaussian heat source is presented in Equation (3), where P is the laser power, A is the laser energy absorption coefficient, and R is the radius at which the energy density is minimized to 1/e2 [19] of the laser intensity at the centre of the laser spot.

$$Q_O(x,y) = \frac{2AP}{\pi R^2} exp\left(\frac{-2\left((x-ut)^2 + y^2\right)}{R^2}\right) \quad (3)$$

The roughness of the as-built sample was introduced to the 3D CAD model of the sample by part modelling, as shown in Figure 2a. The size of the sample taken for 3D modelling was $10 \times 5 \times 0.5$ mm^3. Mesh independency studies were carried out as shown in Figure 2b to select an adequate mesh size for simulation, and mesh with 26,854 elements was used for the analysis. Figure 3 shows the variation in thermophysical properties [20] with temperature.

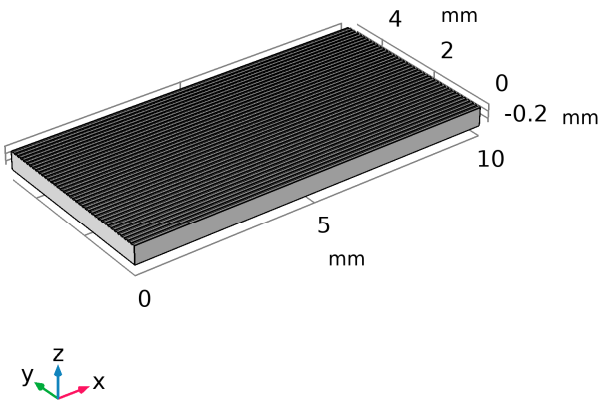

(a)

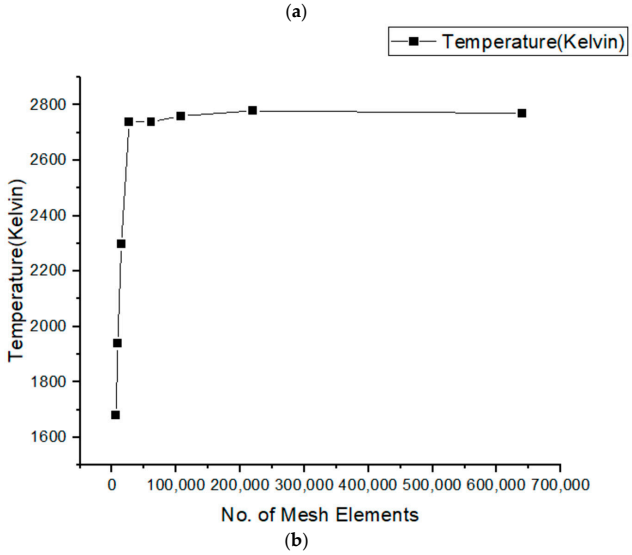

(b)

Figure 2. Numerical modelling of (**a**) 3D model of the sample with surface roughness and (**b**) mesh sensitivity study plot.

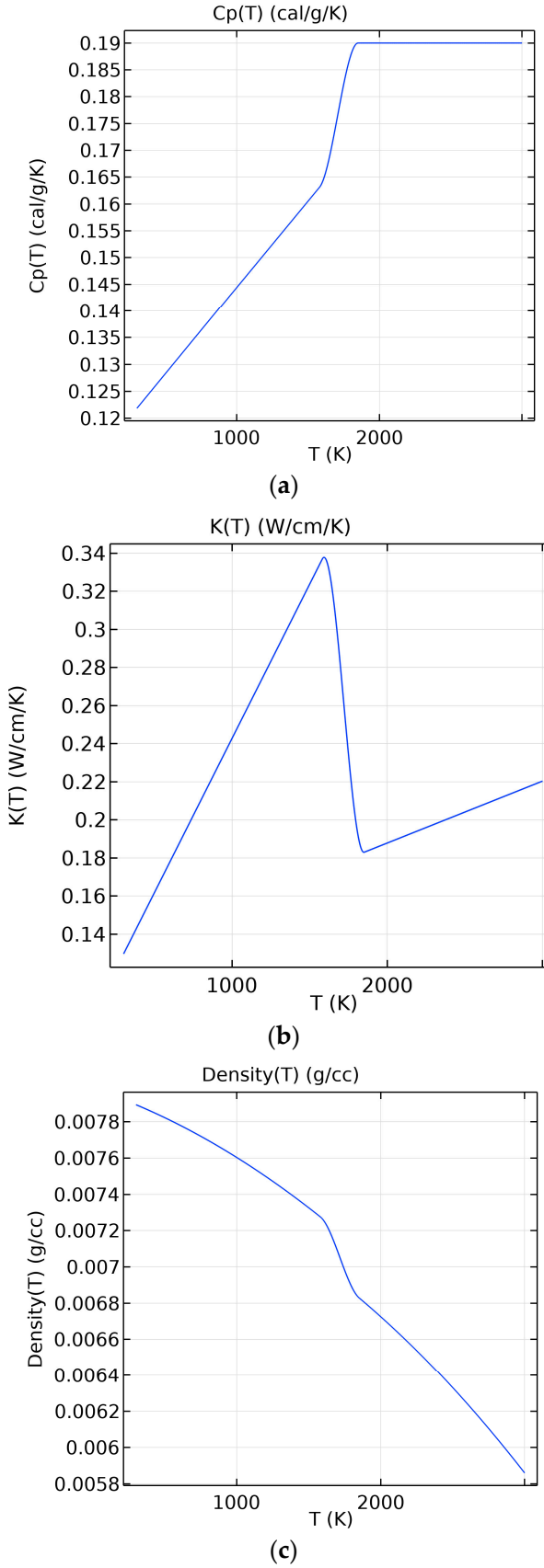

Figure 3. Temperature-dependent (**a**) specific heat, (**b**) conductivity, and (**c**) density [19].

4. Results and Discussion

Figure 4 presents the effect of laser power and scan speed on the melt pool depth based on experimental observations. It was observed that the melt pool depth increased with a rise in laser power and reduced with an increase in the scan speed, which can be explained with LEL. As the laser power increased and scan speed reduced, the LEL value increased, which led to a higher laser energy available per unit length of the material. In addition, the reduction in scan speed increased with increasing interaction time between the laser source and the material. The above factors led to the availability of higher thermal energy, resulting in higher melt pool depth values.

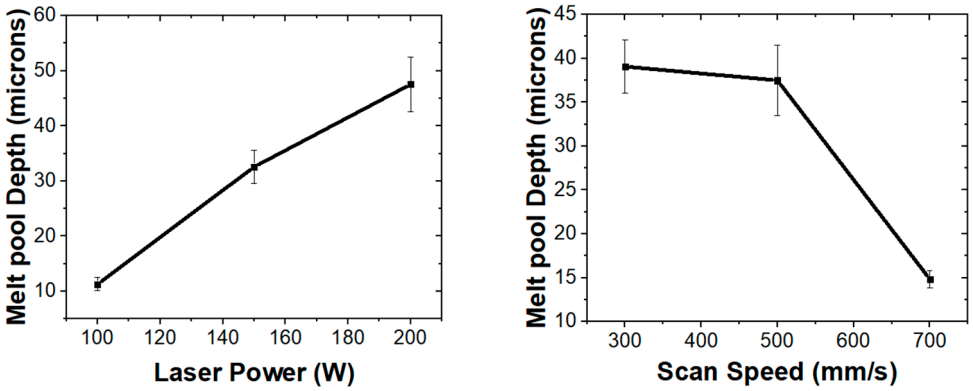

(**a**) (**b**)

Figure 4. Effect of (**a**) laser power and (**b**) scan speed on the mean melt pool depth.

Figure 5 presents the melt pool depth at different values of LEL obtained using experimental studies and numerical simulation. An increasing trend was observed for the melt pool depth with an increase in the LEL. This was mainly due to the availability of more laser energy for melting. A comparison of the simulated melt pool geometry with experimental values, as presented in Figure 5, indicates a maximum deviation of 17.2%. The variation between the experimental results and numerical simulation could be due to various effects, such as spattering, ablation, and the evaporation phenomenon, which were not accounted for in the simulation.

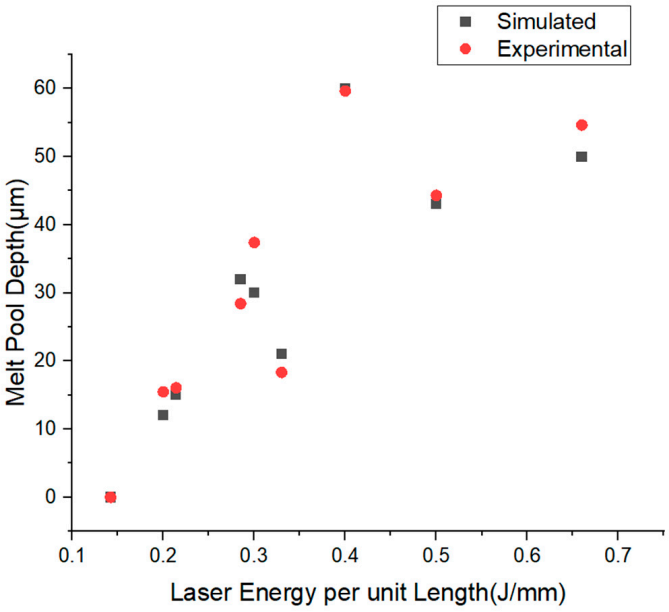

Figure 5. Average melt pool depth values obtained using experimental analysis and numerical simulation.

Figure 6 presents the typical temperature distribution obtained from numerical analysis on the rough surface of the sample obtained through the LDED process and the cross-section image of the sample (from experimental results). The experimental melt pool depth values find a good agreement with the simulation results. It can also be seen from the temperature distribution that the temperature reached a maximum at the centre of the laser beam, and it decreased further away from the centre of the laser beam. This was mainly due to the Gaussian energy distribution of the laser source and faster heater conduction at the edges of the melt pool.

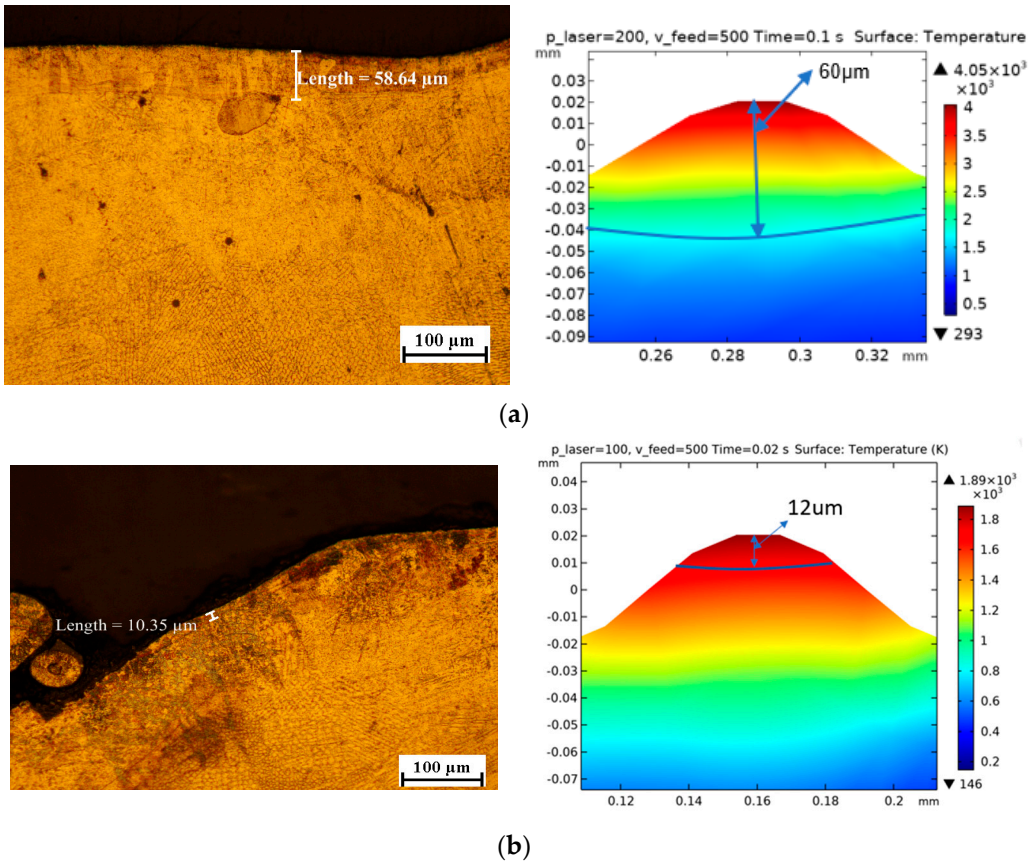

(**a**)

(**b**)

Figure 6. Temperature distribution in experimental and simulated samples at (**a**) LEL = 0.4 J/mm and (**b**) LEL = 0.2 J/mm.

Table 3 presents the experimentally obtained roughness values of samples after laser polishing. The average roughness of the as-built sample was 21.37 µm. A significant reduction in the surface roughness was observed at different process parameters with a minimum surface roughness of 9 µm at a laser power of 150 W and a scan speed of 700 mm/s. Figure 7 presents the variation in surface roughness with respect to laser power and scan speed from the experimental results. The surface roughness initially reduced with an increase in the laser power but increased with an increase in laser power above 150 W. The initial reduction could have been due to the increase in thermal energy available in the melt pool, permitting the melting of unmelted powders on the surface of the LDED-built structure. However, the increase in the surface roughness above a laser power of 150 W could have been due to the excess energy in the melt pool, leading to higher turbulence and over-melting of the surface. On the other hand, an increase in the scan speed reduced the interaction time between the partially melted powder particles and the laser beam. This reduced the amount of thermal energy available at the surface and the conduction of thermal energy, which hindered the complete melting and spreading of the partially melted particles [21].

Table 3. Surface roughness at different laser polishing parameters.

Sample	Laser Power (W)	Scan Speed (mm/s)	LEL (P/V) (J/mm)	Average Roughness (Sa) (μm)
Sample 1	100	300	0.33	11.18
Sample 2	100	500	0.2	13.38
Sample 3	100	700	0.142	16.17
Sample 4	150	300	0.5	12.06
Sample 5	150	500	0.3	14.77
Sample 6	150	700	0.214	9.00
Sample 7	200	300	0.66	14.32
Sample 8	200	500	0.4	13.34
Sample 9	200	700	0.285	17.52
As-Built Sample				21.37

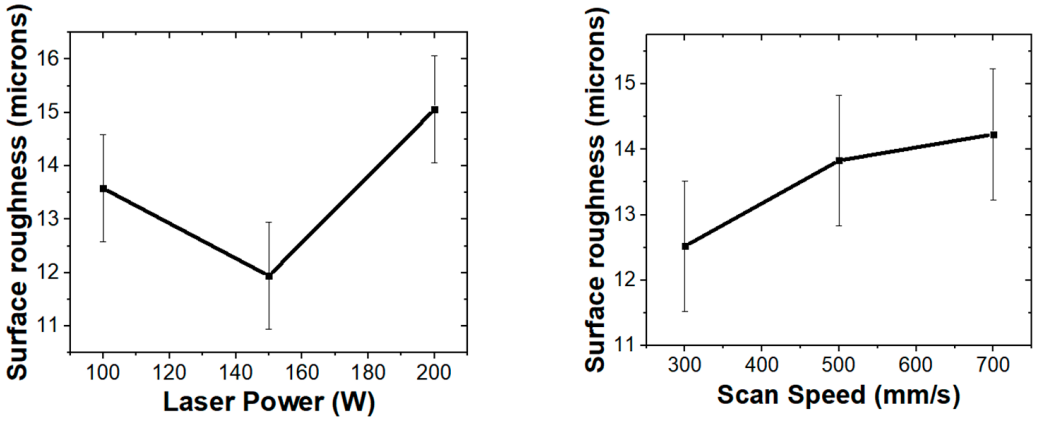

Figure 7. Effect of (**a**) laser power and (**b**) scan speed on the mean surface roughness.

The variation in the surface roughness with process parameters can be explained with the help of shallow surface melting (SSM) and surface over melting (SOM). The SSM area is a partially melted metal surface formed by the capillary pressure created by the shallow melting of micro peaks that fills the valleys with molten metal. The molten metal thickness is smaller than the peak and valley distance in this partially melted metal area. Molten metal flows from peaks to valleys in SSM [10], leading to a reduction in surface roughness as a result of the capillary pressure. However, the melt pool thickness would be more than the peak-to-valley distance at a higher LEL. This results in a decreased frequency of peaks and valleys but an increase in their amplitude, which enhances surface roughness. The region in which the over-melting of the peak occurs is known as SOM [22,23]. Figure 8a represents surface periodic formation during the SOM mechanism. Thus, partially melting the material is always preferred to completely melting it. Therefore, it can be concluded that the surface of the sample underwent three stages when the laser energy increased:

(a) When the laser energy was insufficient to melt the surface, i.e., the incomplete melting zone;
(b) When the laser energy was high enough to melt the material so that it formed an SSM region;
(c) When the laser energy density was too high such that it over-melted the material, i.e., SOM region.

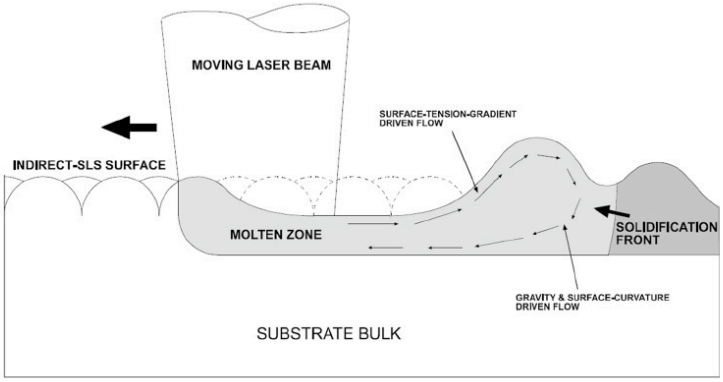

(**a**)

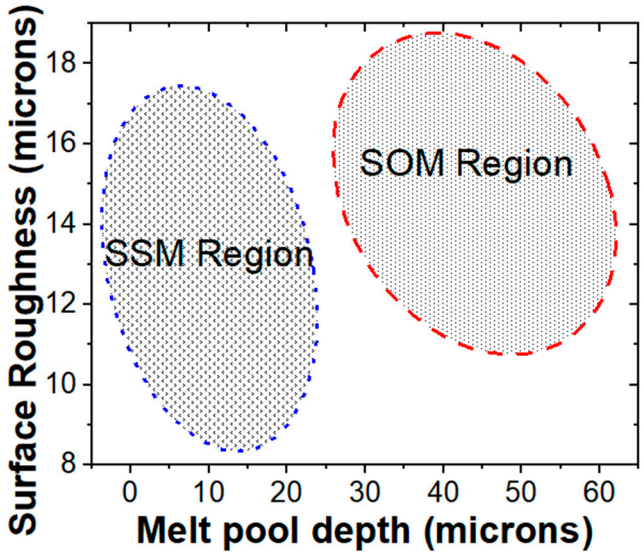

(**b**)

Figure 8. Surface periodic formation (**a**) during SOM mechanism at (**b**) different regions.

The melt pool depth presented previously can be correlated with the surface roughness using SSM and SOM. Figure 8b distinguishes the SOM and SSM modes with respect to the melt pool depth and surface roughness obtained from the experimental results. In SSM, the optimum surface roughness was achieved (9 µm) when the melt depth reached 16.06 µm. The subsequent increase in the melt pool depth resulted in increased surface roughness due to the over-melting as a result of the SOM mode of laser polishing.

The surface profiles of the as-built sample, sample 6, sample 3, and sample 8 are shown in Figure 9a–d, respectively. Sample 6 (LEL = 0.214 J/mm) showed the best surface roughness value among all the samples. Sample 3 (LEL = 0.142 J/mm) and sample 8 (LEL = 0.4 J/mm) showed higher roughness than sample 6 (LEL = 0.214 J/mm). This was due to the lower LEL for sample 3, which was insufficient to melt the peaks, whereas in sample 6, adequate LEL was available to melt the peak into the valley, leading to reduced surface roughness. In the case of sample 7, the LEL was very high, due to which the peak melting rate was so high that the frequency of the peaks decreased, but the amplitude of the new peak increased. It can be noted from Figure 10 that the surface roughness was high when the LEL was low and too high. Similar to Figure 8, SSM and SOM regions can be identified as per the surface roughness value. It is necessary to find the optimum LEL where a lower surface roughness can be achieved. In the present study, the minimum surface roughness was observed at an LEL of 0.214 J/mm, which belongs to the SSM zone.

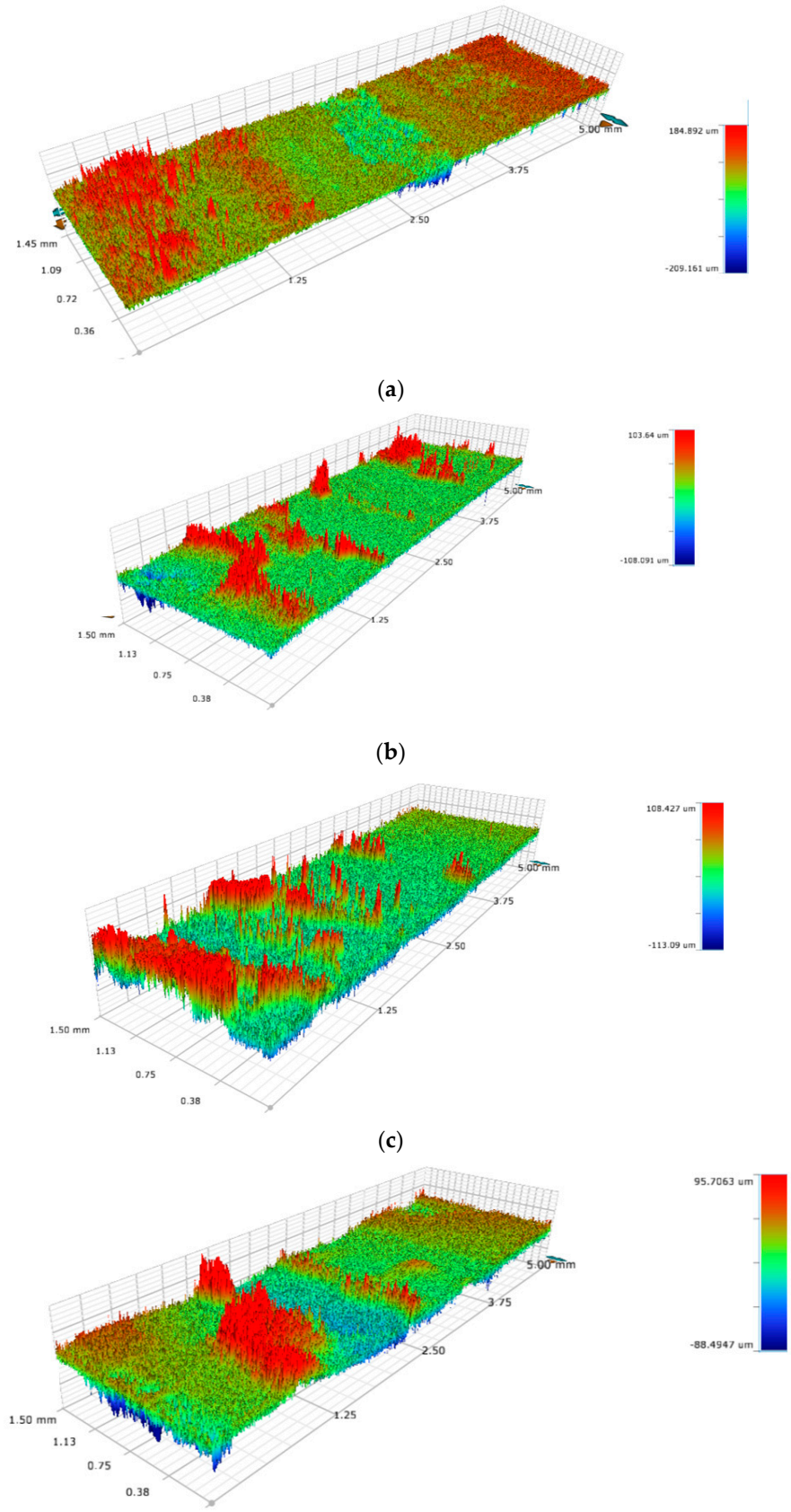

Figure 9. Surface topography of (**a**) as-built samples, (**b**) LEL = 0.214 J/mm, (**c**) LEL = 0.142 J/mm, and (**d**) LEL = 0.4 J/mm.

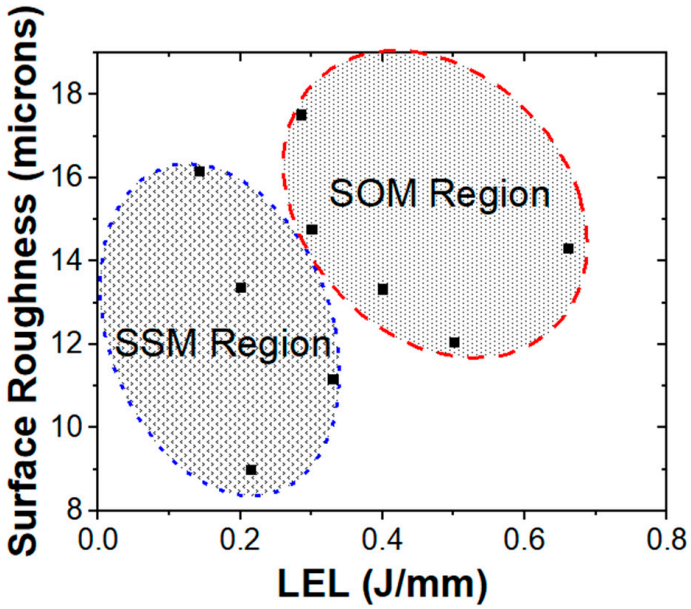

Figure 10. Effect of laser energy per unit length on average surface roughness.

Figure 11 presents the effect of laser polishing on surface topography. Surface topography analysis using SEM showed the presence of partially melted powders on the as-built LDED sample surface (refer to Figure 11a). The balling effect also played a role in increasing the roughness of the as-built sample. The balling effect was caused by powder particles that did not melt or just partially melted and were trapped inside the built layer. The balling effect on the surface of the produced components was caused by insufficient wetting. The partially melted powders were melted by laser polishing, which primarily led to a reduction in the surface roughness of the polished parts. As shown in Figure 11b, a high amount of energy density was available, due to which the presence of irregularities in the melt pool was high. In Figure 11c, no significant effect of laser polishing can be seen since energy density was very low, which resulted in an unmelted regime. However, as seen in Figure 11d, an adequate melting region was formed with minimal existence of the balling effect and irregularities. From the SEM images, it can be concluded that the samples with lower LEL had an unmelted regime, whereas with higher LEL, over-melting and melting irregularities were dominant. At optimum LEL, a smoother surface was obtained due to shallow surface melting.

Figure 12a,b present the elemental mapping of as-built and laser-polished surfaces. It can be seen that the segregation was more evident in the laser-polished samples as opposed to as-built samples. The segregation of Si, Mn, and C was more evident in the samples as they have a higher chance of segregation due to having a lower diffusion coefficient. As shown in Figure 13a, XRD analysis indicated the presence of peaks at angles of 44.42°, 51.58°, 75.47°, and 91.43°corresponding to γ-Fe (111), γ-Fe (200), γ-Fe (220), and γ-Fe (311) [24,25], respectively in as-built samples, along with α(110). It was observed that there was no extra peak on the laser-polished samples. It can also be seen from Figure 13b that a peak shift was observed between the as-built sample and the laser-polished sample. This could have been due to the variation in the lattice spacing as a result of the variation in the lattice strain. In addition, it can also be seen that there was a peak shift between samples polished at different LEL values, which indicates the variation in stress pattern in the material at different LEL values. The crystallite sizes estimated with the Scherrer equation were 52 nm, 49 nm, and 45 nm for 0.66 J/mm, 0.4 J/mm, and 0.285 J/mm, respectively. This indicates that the crystallite size increased with a reduction in the LEL value, which may be attributed to the reduction in the melt pool temperature and higher cooling rates associated with the reduction in LEL during laser polishing at different parameters.

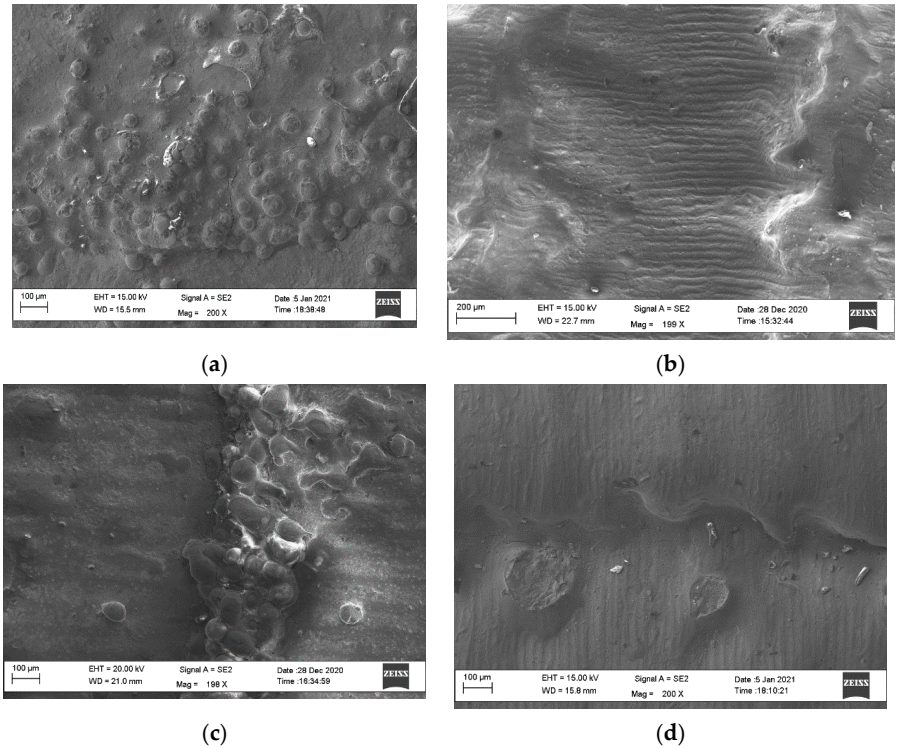

(**a**) (**b**)

(**c**) (**d**)

Figure 11. SEM images of samples (**a**) as-built, (**b**) polished at LEL = 0.33 J/mm, (**c**) polished at LEL = 0.142 J/mm, and (**d**) polished at LEL = 0.214 J/mm.

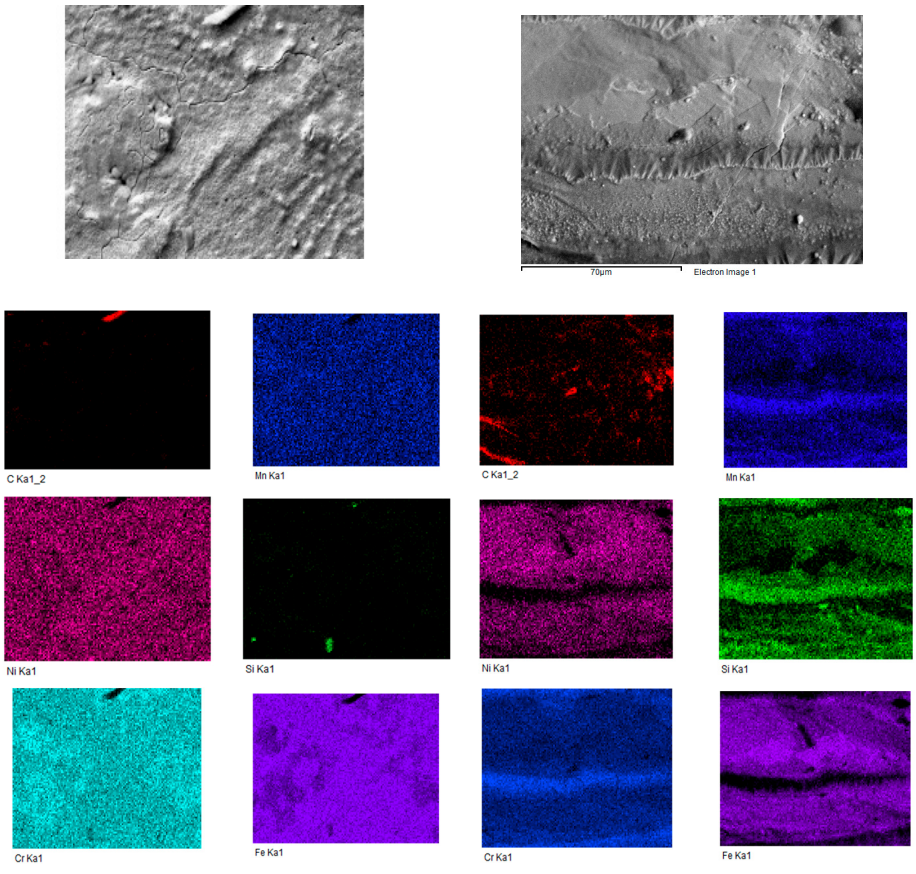

(**a**) (**b**)

Figure 12. EDS mapping of (**a**) as-built and (**b**) laser-polished samples.

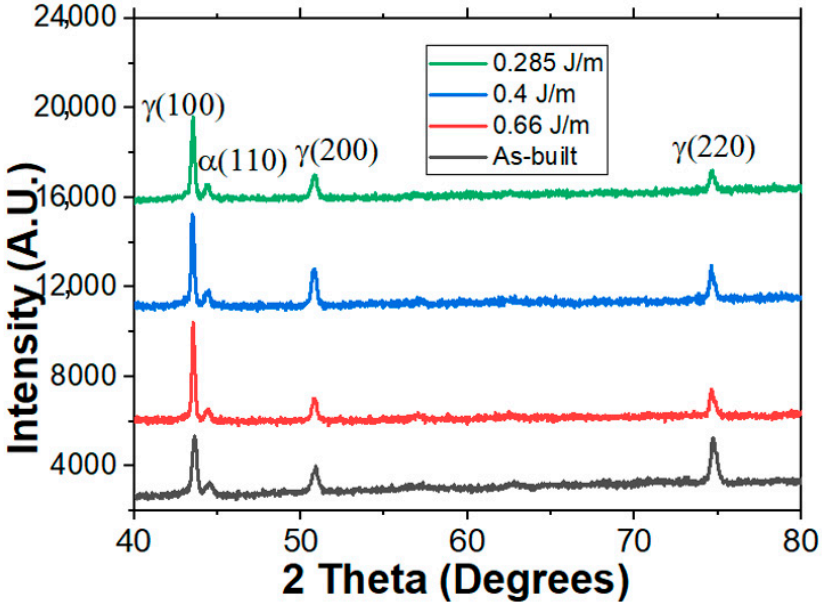

(**a**)

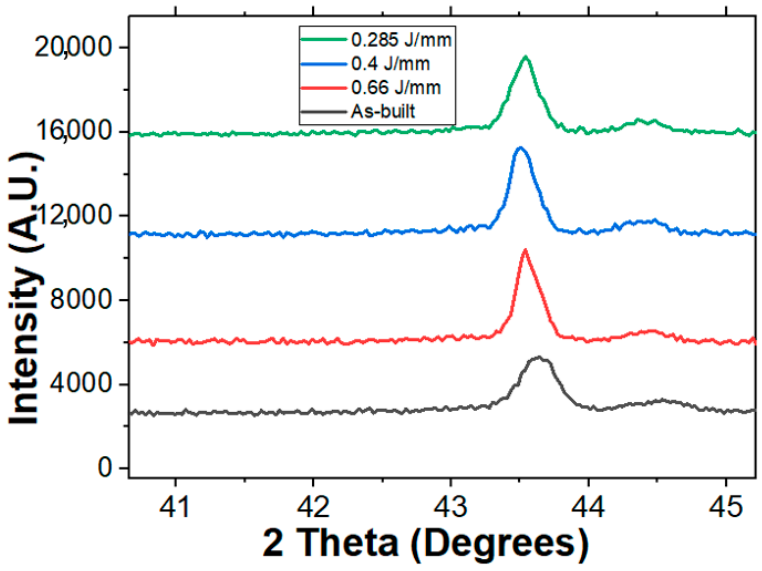

(**b**)

Figure 13. XRD plot of (**a**) as-built sample and laser-polished samples and (**b**) peak shift.

5. Conclusions

In this study, experimental and theoretical studies were carried out on the laser polishing of LDED-built SS 304L samples. The correlation between melt pool simulation and surface roughness was influenced by two phenomena: surface shallow melting (SSM) and surface over-melting (SOM). Both high energy density (ED) and low ED can increase surface roughness, but there exists a region where an optimal roughness can be achieved, lying in the shallow surface melting zone. In this research, a minimum roughness of 9 µm was attained at an ED of 0.214 J/mm. The simulation results for melt pool depth exhibit good agreement with the experimental results, with a maximum deviation of 17%. The experimental findings demonstrate that careful adjustment of process parameters allows for achieving a high-quality surface profile, particularly when the laser energy density falls within the SSM region. SEM analysis reveals that an optimum energy density is crucial, as lower energy density generates a balling effect, while higher energy density leads to over-

melting. SEM-EDS analysis indicates that segregation is more evident in laser-polished samples, and the XRD results reveal no extra peak generation due to laser polishing. However, a peak shift was observed between the as-built sample and the laser-polished sample, possibly due to variations in lattice spacing resulting from lattice strain.

Author Contributions: Conceptualization, J.A.N., N.S. and C.P.P.; methodology, V.K.S., J.A.N. and C.P.P.; formal analysis, V.K.S. and J.A.N.; investigation, V.K.S., J.A.N. and C.P.P.; resources, N.S. and C.P.P.; data curation, V.K.S. and J.A.N.; writing—original draft preparation, V.K.S.; writing—review and editing, J.A.N., N.S. and C.P.P.; supervision, N.S. and C.P.P.; project administration, N.S. and C.P.P.; funding acquisition, N.S. and C.P.P. All authors have read and agreed to the published version of the manuscript.

Funding: Vijay Kumar Saini acknowledges the financial support of a fellowship from the Ministry of Human Resource Development, Government of India, during the above work.

Data Availability Statement: The data presented in this study are available on request from the corresponding author. The data are not publicly available as they are part of ongoing research.

Acknowledgments: The authors thank the members of the Laser Additive Manufacturing Lab, Raja Ramanna Centre for Advanced Technology, Indore, India, for their help in the LDED and laser polishing experiments. The authors acknowledge the support of the Department of Mechanical Engineering and Department of Materials Science and Engineering at the Indian Institute of Technology Kanpur, India, in characterizing the samples.

Conflicts of Interest: The authors declare no conflict of interest.

References

1. Gu, D.; Shi, X.; Poprawe, R.; Bourell, D.L.; Setchi, R.; Zhu, J. Material-Structure-Performance Integrated Laser-Metal Additive Manufacturing. *Science* **2021**, *372*, eabg1487. [CrossRef] [PubMed]
2. Wang, D.; Liu, Y.; Yang, Y.; Xiao, D. Theoretical and Experimental Study on Surface Roughness of 316L Stainless Steel Metal Parts Obtained through Selective Laser Melting. *Rapid Prototyp. J.* **2016**, *22*, 706–716. [CrossRef]
3. Yadav, S.; Jinoop, A.N.; Sinha, N.; Paul, C.P.; Bindra, K.S. Parametric Investigation and Characterization of Laser Directed Energy Deposited Copper-Nickel Graded Layers. *Int. J. Adv. Manuf. Technol.* **2020**, *108*, 3779–3791. [CrossRef]
4. Emdadi, A.; Bolz, S.; Jensch, F.; Tovar, M.; Weiß, S. On the Hot Deformation of a Fe-Al-Ta Iron Aluminide Prepared via Laser Powder Bed Fusion. *Crystals* **2023**, *13*, 627. [CrossRef]
5. Lu, Y.; Zhang, H.; Xue, P.; Wu, L.; Liu, F.; Jia, L.; Ni, D.; Xiao, B.; Ma, Z. Microstructural Evaluation and Tensile Properties of Al-Mg-Sc-Zr Alloys Prepared by LPBF. *Crystals* **2023**, *13*, 913. [CrossRef]
6. Benarji, K.; Kumar, Y.R.; Paul, C.P.; Jinoop, A.N.; Bindra, K.S. Parametric Investigation and Characterization on SS316 Built by Laser-Assisted Directed Energy Deposition. *Proc. Inst. Mech. Eng. Part L J. Mater. Des. Appl.* **2019**, *234*, 452–466. [CrossRef]
7. Strickland, J.D. Applications of Additive Manufacturing in the Marine Industry. In Proceedings of the 13th International Symposium on Practical Design of Ships and Other Floating Structures (PRADS) 2016, Copenhagen, Denmark, 4–8 September 2016. [CrossRef]
8. Izadi, M.; Farzaneh, A.; Mohammed, M.; Gibson, I.; Rolfe, B. A Review of Laser Engineered Net Shaping (LENS) Build and Process Parameters of Metallic Parts. *Rapid Prototyp. J.* **2020**, *26*, 1059–1078. [CrossRef]
9. Bhaduri, D.; Penchev, P.; Batal, A.; Dimov, S.; Soo, S.L.; Sten, S.; Harrysson, U.; Zhang, Z.; Dong, H. Laser Polishing of 3D Printed Mesoscale Components. *Appl. Surf. Sci.* **2017**, *405*, 29–46. [CrossRef]
10. Krishnan, A.; Fang, F. Review on Mechanism and Process of Surface Polishing Using Lasers. *Front. Mech. Eng.* **2019**, *14*, 299–319. [CrossRef]
11. Ermergen, T.; Taylan, F. Review on Surface Quality Improvement of Additively Manufactured Metals by Laser Polishing. *Arab. J. Sci. Eng.* **2021**, *46*, 7125–7141. [CrossRef]
12. Marimuthu, S.; Triantaphyllou, A.; Antar, M.; Wimpenny, D.; Morton, H.; Beard, M. Laser Polishing of Selective Laser Melted Components. *Int. J. Mach. Tools Manuf.* **2015**, *95*, 97–104. [CrossRef]
13. Dadbakhsh, S.; Hao, L.; Kong, C.Y. Surface Finish Improvement of LMD Samples Using Laser Polishing. *Virtual Phys. Prototyp.* **2010**, *5*, 215–221. [CrossRef]
14. Hafiz, A.M.K.; Bordatchev, E.V.; Tutunea-Fatan, R.O. Influence of Overlap between the Laser Beam Tracks on Surface Quality in Laser Polishing of AISI H13 Tool Steel. *J. Manuf. Process* **2012**, *14*, 425–434. [CrossRef]
15. Souza, A.M.; Ferreira, R.; Barragán, G.; Nuñez, J.G.; Mariani, F.E.; da Silva, E.J.; Coelho, R.T. Effects of Laser Polishing on Surface Characteristics and Wettability of Directed Energy-Deposited 316L Stainless Steel. *J. Mater. Eng. Perform.* **2021**, *30*, 6752–6765. [CrossRef]

16. Paul, A.C.; Jinoop, A.N.; Paul, C.P.; Deogiri, P.; Bindra, K.S. Investigating Build Geometry Characteristics during Laser Directed Energy Deposition Based Additive Manufacturing. *J. Laser Appl.* **2020**, *32*, 42002. [CrossRef]
17. Nayak, S.K.; Jinoop, A.N.; Paul, C.P.; Kumar, V.A.; Subburaj, D.; Singh, R.; Bindra, K.S. On the Hot Isostatic Pressing of Inconel 625 Structures Built Using Laser Powder Bed Fusion at Higher Layer Thickness. *Int. J. Adv. Manuf. Technol.* **2022**, *120*, 4065–4078. [CrossRef]
18. Ansari, M.J.; Nguyen, D.-S.; Park, H.S. Investigation of SLM Process in Terms of Temperature Distribution and Melting Pool Size: Modeling and Experimental Approaches. *Materials* **2019**, *12*, 1272. [CrossRef]
19. Mohajerani, S.; Miller, J.D.; Tutunea-Fatan, O.R.; Bordatchev, E. V Thermo-Physical Modelling of Track Width During Laser Polishing of H13 Tool Steel. *Procedia Manuf.* **2017**, *10*, 708–719. [CrossRef]
20. Kim, C.S. *Thermophysical Properties of Stainless Steels*; Argonne National Laboratory: Lemont, IL, USA, 1975.
21. Liu, S.; Guo, H. Balling Behavior of Selective Laser Melting (SLM) Magnesium Alloy. *Materials* **2020**, *13*, 3632. [CrossRef]
22. Ramos, J.A.; Bourell, D.L.; Beaman, J.J. Surface Over-Melt During Laser Polishing of Indirect-SLS Metal Parts. *MRS Online Proc. Libr.* **2003**, *758*, 19. [CrossRef]
23. Ukar, E.; Lamikiz, A.; Lopez De Lacalle, L.N.; Del Pozo, D.; Liebana, F.; Sanchez, A. Laser Polishing Parameter Optimisation on Selective Laser Sintered Parts. *Int. J. Mach. Mach. Mater.* **2010**, *8*, 417–432. [CrossRef]
24. Modiri, F.; Savaloni, H. A Study of the Corrosion of Stainless Steel 304L Coated with a 190 Nm-Thick Manganese Layer and Annealed with Nitrogen Flux in a 0.4-Mole Solution of H_2SO_4 at Different Temperatures. *J. Theor. Appl. Phys.* **2020**, *14*, 21–35. [CrossRef]
25. Singh, R.; Sharma, S.; Vajpai, S.K. Effect of Reversible Cyclic Plastic Deformation and Thermal Treatment on the Microstructure and Mechanical Properties of SS304L Steel. *Trans. Indian Inst. Met.* **2020**, *73*, 1227–1237. [CrossRef]

Disclaimer/Publisher's Note: The statements, opinions and data contained in all publications are solely those of the individual author(s) and contributor(s) and not of MDPI and/or the editor(s). MDPI and/or the editor(s) disclaim responsibility for any injury to people or property resulting from any ideas, methods, instructions or products referred to in the content.